



PERGAMON

Journal of Atmospheric and Solar-Terrestrial Physics 60 (1998) 907–915

Journal of
ATMOSPHERIC AND
SOLAR-TERRESTRIAL
PHYSICS

Spectrum of red sprites

G. Milikh^{a,*}, J. A. Valdivia^b, K. Papadopoulos^{a,b}

^aDepartment of Astronomy, ^bDepartment of Physics, University of Maryland, College Park MD 20742, U.S.A.

Received 16 December 1996; accepted 11 February 1998

Abstract

A synthetic spectrum of red sprites due to electron energization by the electric field from lightning is presented. It is computed by using the electron distribution function obtained from a Fokker–Planck code, which includes various inelastic losses. The model also includes the atmospheric attenuation of the optical emissions. The results are compared with observed red sprite spectra. Some implications of the results to models of red sprites are discussed. © 1998 Elsevier Science Ltd. All rights reserved.

1. Introduction

Observations of optical emissions at altitudes between 60–90 km associated with giant thunderstorms have been the focus of many recent ground and aircraft campaigns (Lyons, 1994; Sentman et al., 1995; Winckler et al., 1996). While the gross phenomenology of the emissions, termed red sprites, has been known for some time now, their spectroscopic structure is only currently emerging (Mende et al., 1995; Hampton et al., 1996). The objective of this paper is to present a model of the optical spectrum of red sprites due to the electron energization by lightning-induced electric fields. A valuable output of such a model is the scaling of the relative intensities of the emissions with the value of the electric field and/or power density of the energy deposition. Such scaling can provide additional constraints to the required energy deposition in the red sprite region.

2. Model description

The model assumes energization of ionospheric electrons by fields generated by conventional lightning and applies equally well to energization by electro-magnetic or quasi-static fields (Milikh et al., 1995; Rowland et al., 1995; Pasko et al., 1995). It capitalizes on the fact that there are two distinct timescales—a short timescale on

which a steady state electron distribution function $f(v)$ is established by balancing the electron energization rate with inelastic losses (Tsang et al., 1991), and a longer radiation timescale dominated by interlevel transfer and collisional quenching. A Fokker–Planck code that includes elastic and inelastic collisions (Tsang et al., 1991) is used to calculate the electron energization at altitudes between 60–90 km by lightning generated fields with frequency ω smaller than the electron cyclotron frequency Ω_e and the electron–neutral collisional frequency ν_0 . It computes kinetically the modification of the electron distribution function by the field and the excitation of the molecular electronic levels by the energized electrons. Radiative de-excitation of the excited molecules produced optical flashes that superficially resemble those observed during auroras. However, unlike auroras which last for hours and in which even forbidden transitions need to be considered, red sprites have durations of only milliseconds, so that only N_2 transitions less than a millisecond, excited by direct electron impact or through cascades, need to be retained. Finally the emission spectrum at ground or airplane level is computed by including the atmospheric attenuation.

2.1. Electron distribution function

The electron distribution function in the presence of an electric field is strongly non-Maxwellian requiring a kinetic treatment of the problem. This provides the value of the electron–neutral collisional frequency $\nu_e = \nu_e(z, |E|)$, and the excitation rates of the different electronic levels by electron impact. An existing Fokker–

* Corresponding author. E-mail: milikh@astro.umd.edu

Planck code, developed for the description of ionospheric RF breakdown (Tsang et al., 1991) was used. The basic input to the model is the electric field amplitude E at a particular altitude z characterized by the ambient electron–neutral collisional frequency ν_0 . Here E is defined as $E = \sqrt{\Sigma E_\omega^2}$, where E_ω^2 is the spectral energy density. This definition of electric field amplitude is general and applies to quasi-static or electromagnetic fields for $\omega \ll \Omega_e, \nu_e$. For a given value of E and ν_0 , the electron distribution function $f(v)$ is found by solving numerically the Fokker–Planck equation

$$\frac{\partial f}{\partial t} - \frac{1}{3mv^2} \frac{\partial}{\partial v} \left(v^2 \nu_e(v) \tilde{\varepsilon}(E, \nu_e(v)) \frac{\partial f}{\partial v} \right) = \mathcal{L}(f), \quad (1)$$

where

$$\tilde{\varepsilon}(E, \nu) = \frac{e^2 E^2}{m[\Omega_e^2 + \nu_e^2]} \left\{ 1 + \left(\frac{\Omega_e}{\nu_e} \right)^2 \cos^2 \theta_0 \right\}$$

is the electron quiver energy, and $\nu_e(v)$ is the electron–neutral effective collisional frequency. \mathcal{L} is the operator which describes the effect of the inelastic collisions (Tsang et al., 1991). We have assumed that the frequency of the electromagnetic fields satisfy $\omega \ll \Omega_e, \nu_e$ and that the magnetic field is almost perpendicular to the E field so that $(\Omega_e/\nu_e)^2 \cos^2 \theta_0 \ll 1$. The critical parameter that controls the behavior of the distribution function $f(v)$ under an electric field E at a given height is the averaged quiver energy $\tilde{\varepsilon}(E, \nu_e)$, which depends nonlinearly on the steady state averaged collisional frequency, ν_e . For values of $\tilde{\varepsilon} < 0.02$ eV most of the energy absorbed by the electrons excites the low lying vibrational levels of nitrogen, and emissions in the visible range cannot be excited. For 0.02 eV $< \tilde{\varepsilon} < 0.1$ eV the electron energy results in the excitation of optical emissions and molecular dissociation. For $\tilde{\varepsilon} > 0.1$ eV ionization is initiated.

2.2. Computing the radiative intensity

The next element of the model is the computation of the emission intensity for a particular radiative transition based on the value of $f(v)$ found above. In the current model we have retained only the electronic levels of N_2 shown in Fig. 1. The computation of the intensity of a radiative transition connecting the v -th and v' -th vibrational levels of electronic states α and β is accomplished as follows. We first compute the excitation rate k_{ex}^α coefficient of the α electronic level of N_2 by electron impact

$$k_{\text{ex}}^\alpha = 4\pi \int f(v) v^3 \sigma_{\text{ex}}^\alpha(v) dv,$$

using the excitation cross-section $\sigma_{\text{ex}}^\alpha$ of the B, B', W, C and E electronic levels by the electron impact from Cartwright et al. (1977), while the excitation cross-section of the $N_2(\text{D})$ electronic level is taken from Freund (1971)

and normalized by using the peak value from Cartwright (1970). The excitation cross-section of the $N_2^+(\text{B})$ electronic level by the electron impact from the ground state was taken from Van Zyl and Pendleton (1995). Note that k_{ex}^α only depends on the quiver energy $\tilde{\varepsilon}$.

Figure 2 shows the excitation rate coefficients for the relevant electronic levels of N_2 as a function of the quiver energy $\tilde{\varepsilon}$. We have neglected effects caused by the $W \rightarrow B$ transition compared with that due to $B \rightarrow B'$ transition, both having similar excitation thresholds but different excitation rates as revealed by Fig. 2. We then obtain the population of vibrational levels inside each of the electronic states by solving the following set of stationary equations (Cartwright, 1978)

$$\begin{aligned} \frac{dn_v^\alpha}{dt} &= q_{0v}^{\alpha\alpha} K_{\text{ex}}^\alpha N_{N_2} n_e + \sum_{\beta j} A_{jv}^{\alpha\beta} n_j \\ &\quad - n_v^\alpha \sum_{\beta j} A_{vj}^{\alpha\beta} - k_{q,v}^\alpha N n_v^\alpha = 0, \end{aligned} \quad (2)$$

where:

- n_e is the electron density,
- n_v^α is the number density of the v -th vibrational level of electronic state α ,
- $q_{0v}^{\alpha\alpha}$ is the Franck–Condon factor which shows the transition probability to the v vibrational level of the α electronic state from the 0 vibrational level of the ground state X (in a cold ambient gas only the lowest vibrational level is populated),
- $A_{vv}^{\alpha\beta}$ is the Einstein spontaneous transition probability,
- $k_{q,v}^\alpha$ is the rate constant of collisional quenching of the v vibrational level of the α electronic state,
- N is the air density.

Therefore, the first term in the right side of eqn (2) shows the direct pumping of the v vibrational level of the α electronic state by the electron impact. While the second term shows cascade excitation, the third term describes the radiation losses. The last term reveals losses due to the collisional quenching. Note that the usage of the stationary equations for the population of vibration levels is justified by the fact that the radiative lifetimes of the relevant electronic states are shorter than the duration T of electromagnetic pulse from lightning in order to be pumped effectively. Therefore, a stationary distribution of n_v^α is established during the pulse. From eqn (2) we obtain the population of the electronic level α as

$$\begin{aligned} n_v^\alpha &= N_{N_2} n_e \left(k_{\text{ex}}^\alpha F_{1,v}^\alpha + \sum_{\beta} k_{\text{ex}}^\beta F_{2,v}^{\beta\alpha} \right), \\ F_{1,v}^\alpha &= \frac{q_{0v}^{\alpha\alpha}}{1 + \tau_v^\alpha k_{q,v}^\alpha N}, \\ F_{2,v}^{\beta\alpha} &= \frac{\tau_v^\alpha}{1 + \tau_v^\alpha k_{q,v}^\alpha N} \sum_j F_{1,j}^\beta A_{jv}^{\alpha\beta}. \end{aligned} \quad (3)$$

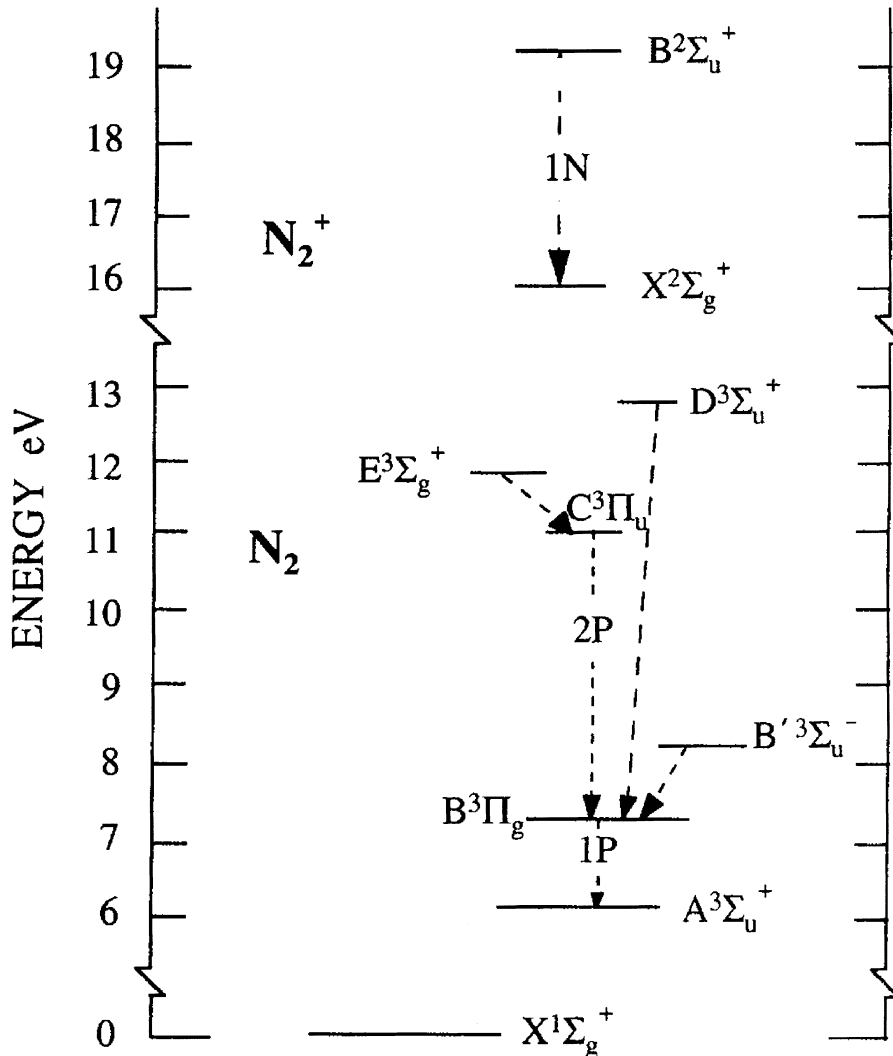


Fig. 1. Energy levels diagram for the nitrogen electronic levels considered in the discussed model. The relevant radiative transitions are shown by arrows.

Here $\tau_v^\alpha = 1/\sum_{j\beta} A_{vj}^{\alpha\beta}$ is the lifetime of the v -th vibrational level of the α electronic state. The coefficients $F_{1,v}^\alpha$ and $F_{2,v}^\beta$ reveal relative importance of the direction and cascade excitation of v -th vibrational level of state α , and are calculated using the data from Gilmore et al. (1992). Moreover, the quenching factor $(1 + \tau_v^\alpha k_{q,v}^\alpha N)^{-1}$ was calculated for the relevant electronic levels using the quenching rate coefficient recently revised by Morill and Benesh (1996) and the quenching rates of $N_2^+(B)$ from Pancheshnyi et al. (1997), see Fig. 3.

Note that collisional transfer between the $N_2(B)$ and other excited N_2 states could affect the N_2 optical spectrum (Morill and Benesh, 1996) and is an important issue for quasistationary auroras. The collisional transfer of excitation which couples resonant vibrational levels of

overlapping B, A, W and B' electronic states of N_2 could affect sprite spectra at the height where this process occurs on a time scale shorter than the sprite duration (Morill and Benesh, 1996). This effect will be considered in a complete model which will be presented elsewhere. The intensity of the radiative transition in Rayleighs' connecting the v -th and v' -th vibrational levels of electronic states α and β is given by

$$I_{vv'}^{\alpha\beta}(\lambda) = \frac{10^{-6}}{4\pi} \int n_v^\alpha A_{vv'}^{\alpha\beta} dl, \quad (4)$$

where the integration is carried out along the optical path of the detector (column integrated). Note that, since we are interested in the relative intensities, we can construct

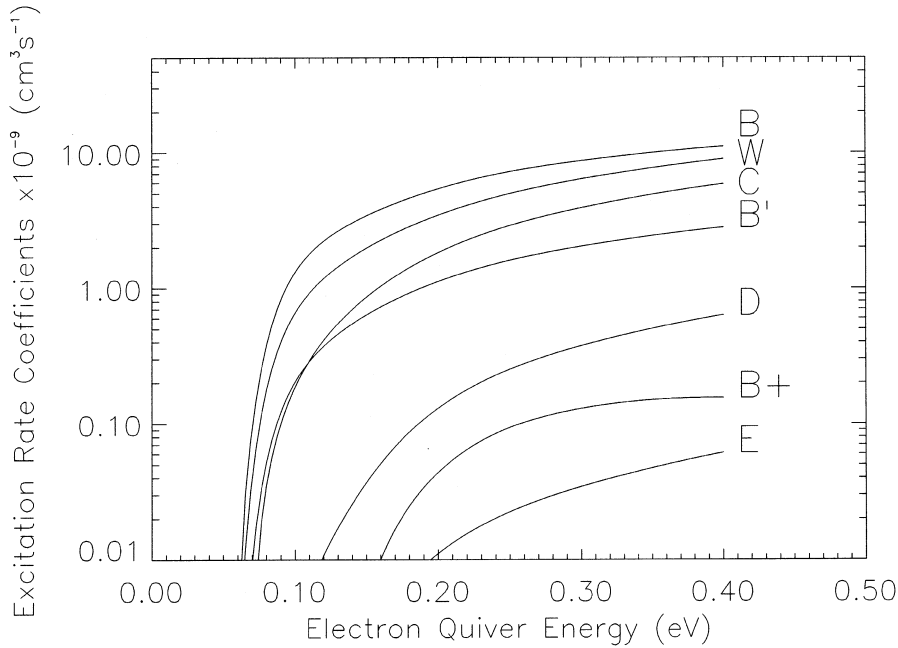


Fig. 2. The excitation rate coefficients for the different levels B, B', W, C, E of the neutral molecular nitrogen, along with the B level of the nitrogen ion, marked as B⁺.

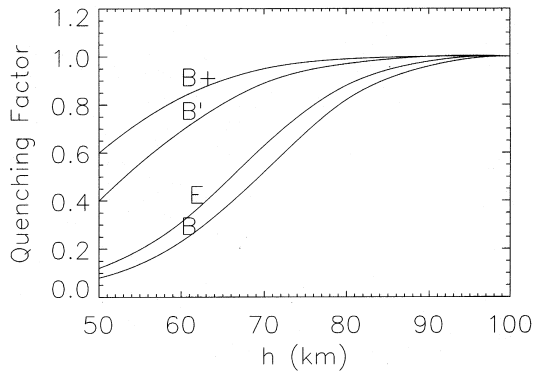


Fig. 3. The effective quenching factor for the electronic levels of (B, B', E, B⁺) as a function of altitude.

a spectrum, at a given height, that depends only on the quiver energy $\tilde{\epsilon}$ as long as quenching is not considered. The vibrational-electronic population depends linearly on the electron density [see eqn (3)]; as a result the spectrum is not affected by the possible increase in the electron density due to the ionization of the neutral gas by 'hot' electrons.

2.3. Atmospheric attenuation

The observed spectrum depends on the location of the detector. If observed from space, the spectrum is the same as the source spectrum, while if observed from either the

ground or an airplane it will be distorted by atmospheric attenuation. Atmospheric attenuation depends on the zenith angle χ of the optical source, the altitude h_0 of the detector, and on the properties of the atmosphere, such as relative humidity and aerosol density. We consider the following contributions to the attenuation: absorption by ozone, oxygen and water vapor, the Rayleigh scattering by air molecules, and Mie scattering by aerosols. The total attenuation of the optical emission is the result of the above contributions and is given by

$$I(h, \chi, \epsilon, \lambda) = I_s(\epsilon, \lambda) e^{-\tau(h, \chi, \epsilon, \lambda)}$$

$$\tau(h, \chi, \epsilon, \lambda) = -\sec \chi \sum_s \sigma_{\text{abs}}^s(\lambda) \int_h^{h_0} N_s(z) dz, \quad (5)$$

where h_0 is the altitude of the sprite, I_s is the sprite source spectrum discussed in the next section, $\sigma_{\text{abs}}^s(\lambda)$ is the corresponding effective attenuation cross-section, and $N_s(z)$ is the density of particles that absorb or scatter the photons. Important points are as follows:

- The absorption by molecular oxygen is computed by taking into consideration the fact that the absorption of O₂ has four narrow peaks centered at $\lambda = 687.2, 689.3, 760.8$ and 763.8 nm (Greenblatt et al., 1990).
- The absorption by ozone is computed using the absorption cross-section from Lenoble (1993), and applying the mid-latitude ozone model (Brasseur and Solomon, 1984).

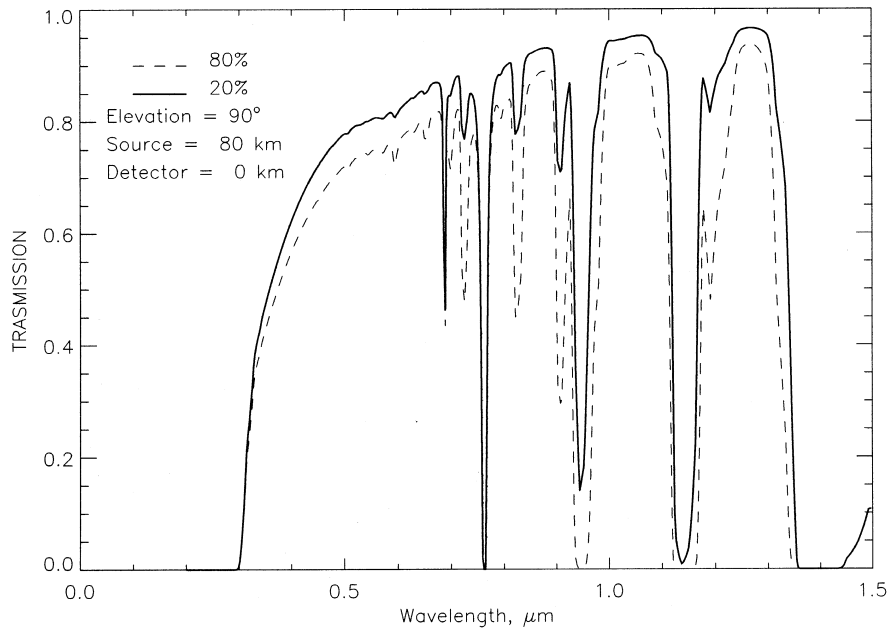


Fig. 4. The transmission coefficient for the atmospheric attenuation model, for two values of the humidity, 80% (lower curve) and 20% (top curve), with $\chi = 0$.

- The absorption caused by the water vapor is calculated using the cross-section from Lenoble (1993). We assume 80% relative humidity, take the dependence of the water vapor pressure on the temperature from the Handbook of Chemistry and Physics (1983, Fig. 18-13), and assume also that the temperature in the troposphere follows the profile observed at Wallops Island (38N°) during summer time (Handbook of Geophysics, 1985, Fig. 15-13).
- The Rayleigh scattering was calculated using the wavelength dependence of the cross-section given by Nicolet et al. (1982).
- Finally, the Mie scattering was calculated by assuming the vertical distribution of the aerosol attenuation (at 0.55 μm) from the background spring–summer model (Handbook of Geophysics, 1985, pp. 18-13). We then extend the attenuation to any wavelength by using the tropospheric aerosol model (Handbook of Geophysics, 1985, Fig. 18-21).

For the sake of definiteness, we assumed in general 80% humidity and 5000 particles/cm³ number density of aerosols. As an example, the transmission coefficient $e^{-\tau(h,\chi,\epsilon,\lambda)}$ is plotted in Fig. 4 for the observational parameters described in the caption and figure.

3. Results

Using the above computational scheme we find next the synthetic source spectrum of N₂. We assume first that

sprites are located at a certain height z , and for the sake of definiteness assume that $z = 80$ km. Then we discuss a more realistic model of a spatially integrated spectrum of red sprites.

Even though the source spectrum depends on the quiver energy and spatial profile of the emission region, which can only be obtained from a specific lightning model, we can estimate the importance of the three given bands by computing the number of band integrated photons as a function of quiver energy, as shown in Fig. 5 assuming that the sprite is located at 80 km. These values can be used to estimate an absolute emission spectrum.

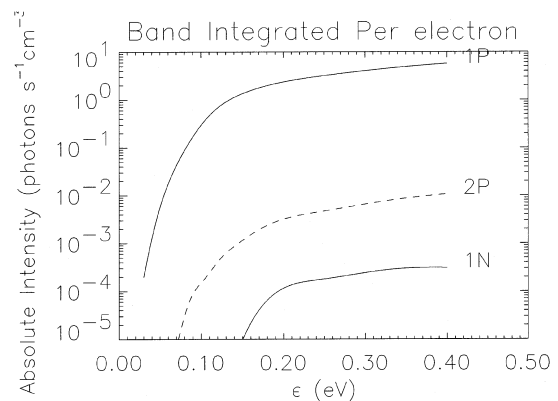


Fig. 5. The band integrated photons as a function of quiver energy for the three bands. The sprite height was assumed at 80 km.

Once we have the source spectrum we consider the model spectrum at the ground observed at different zenith angles. By comparing the model spectrum with observations we estimate the intensity of the pumping electric field.

3.1. Localized-source spectrum

Here we consider a localized source spectrum with and without atmospheric attenuation effects. The synthetic source spectrum of N_2 at a reference height of 80 km is obtained for quiver energies $\tilde{\epsilon} = 0.1$ and 0.2 eV (see Fig. 6) which corresponds to an electric field amplitude $E_0 = 35$ and 70 V/m.

Notice that only the 1P and 2P bands give a distinctive contribution to the source spectrum, while the $N_2^+(1N)$ band plays only a minor role since it can be excited by 'tail' electron having energy in excess of 19 eV. The intensity of the band was still insignificant when we computed it using an electric field a few times higher than mentioned above. In comparison, this $N_2^+(1N)$ band is among the brightest in auroras since it is caused by high energy electrons. Figure 7 reveals the model sprite spectrum at sea level if a ground based detector views the source at zero zenith angle $\chi = 0$. This spectrum differs significantly from the synthetic source spectrum of Fig. 6. First, the $N_2(2P)$ and $N_2^+(1N)$ bands are attenuated more significantly than the $N_2(1P)$ band. This effect is stronger for longer optical paths corresponding to higher zenith angles, as seen in Fig. 8. By comparing the two peaks of the $N_2(1P)$ band, say 5-2 and 4-2 which undergo different absorption, one can estimate the zenith angle of the observed sprite.

Finally, the synthetic spectrum calculated for $\tilde{\epsilon} = 0.1$ eV and zenith angle of $\chi = 80^\circ$, and for the detector location of 4.3 km above sea level, which is shown in Fig. 9(b), resembles that observed by Hampton et al. (1996) at similar conditions, as revealed by Fig. 9(a). From the optical spectrum one can retrieve the intensity of the

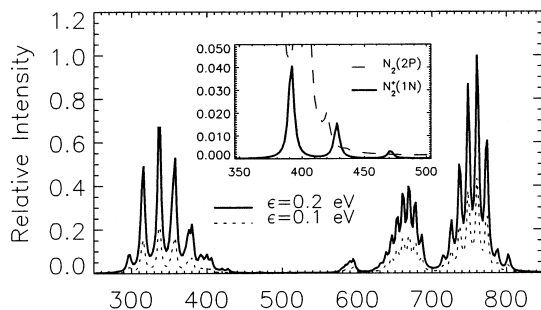


Fig. 6. The source spectrum for $\tilde{\epsilon} = 0.1$ and 0.2 eV, which corresponds to $E_0 = 35$ and 70 V/m assuming a height $h = 80$ km. Also shown is a zoom of the $N_2^+(1N)$ band for $\tilde{\epsilon} = 0.2$, showing that its contribution is small for this range of electron energies.

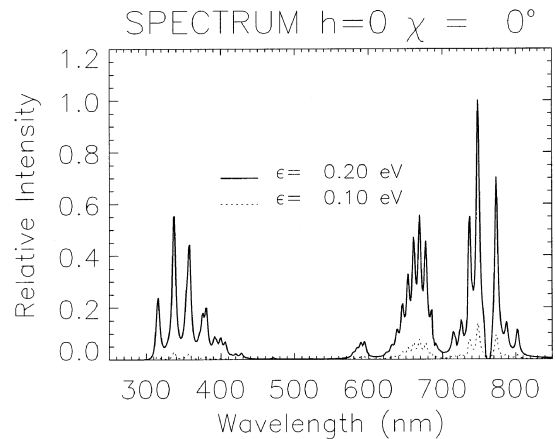


Fig. 7. The sprite spectrum, produced at $h = 80$ km, as it would be observed at the ground with $\chi = 0^\circ$ and for $E_0 = 35$ and 70 V/m, corresponding to $\tilde{\epsilon} = 0.1$ and 0.2 eV, respectively.

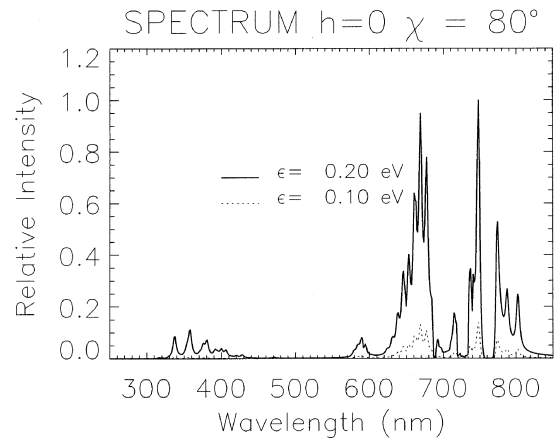


Fig. 8. The sprite spectrum, produced at $h = 80$ km, as it would be observed at the ground with $\chi = 80^\circ$ and for $E_0 = 35$ and 70 V/m, corresponding to $\tilde{\epsilon} = 0.1$ and 0.2 eV, respectively. The relative attenuation of the $N_2(2P)$ and $N_2^+(1N)$ bands as compared with the $N_2(1P)$ band is clearly more significant as χ increased.

pumping electric field. This is accomplished by comparing lines either belonging to different bands or to the same band. In the first case the ratio of excitation rates of the corresponding electronic levels depends on the direct pumping of the levels (mainly) and from cascades' excitation. In the second case this ratio is controlled by the cascades' excitation only. Since only a few lines belonging to the 1P band have been observed so far (Mende et al. 1995; Hampton et al., 1996), in what follows we consider the vibrational transitions $v-v'$ and $v_1-v'_1$ belonging to the $N_2(1P)$ band. For given values of the relative intensities of the two chosen spectral lines $I_{vv'}$ and $I_{v_1v'_1}$ we find using eqns (3) and (4), that

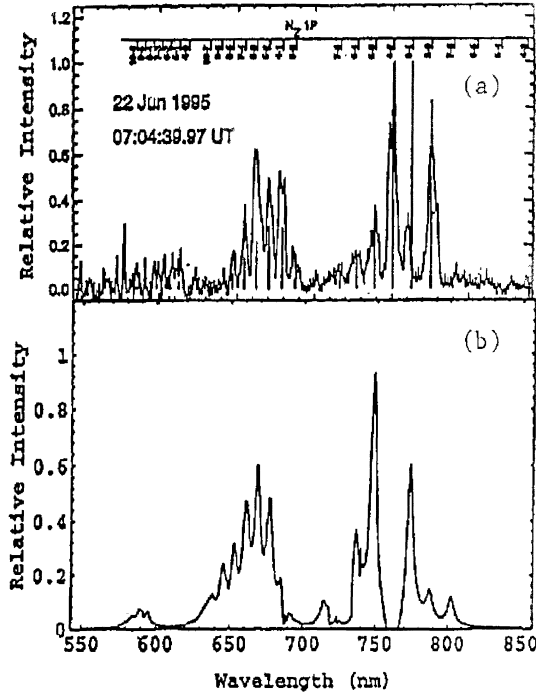


Fig. 9. (a) The spectrum measured by Hampton et al. (1996), with $\chi = 80^\circ$. (b) The modeled spectrum for the estimated $E_0 = 35$ V/m, or $\tilde{\varepsilon} = 0.1$ eV, which is close to the ionization threshold, was computed for the same conditions as for the spectrum shown in (a).

$$\frac{I_{v'v'}}{I_{v_1v_1'}} = \frac{A_{v'v'}}{A_{v_1v_1'}} \frac{v_{\text{ex}}^B F_{1,v'} + \sum_{\alpha} v_{\text{ex}}^{\alpha} F_{2,v'}}{v_{\text{ex}}^B F_{1,v_1'} + \sum_{\alpha} v_{\text{ex}}^{\alpha} F_{2,v_1'}} e^{-(\tau_{v'v'} - \tau_{v_1v_1'})} \quad (6)$$

where the summation is over B', C and D electronic states reflecting the effect of excitation and cascade; $\tau_{v'v'}$ and $\tau_{v_1v_1'}$ reveal the atmospheric absorption of the corresponding levels. Generally speaking, one can obtain the ratios $v_{\text{ex}}^{B'}/v_{\text{ex}}^B$, $v_{\text{ex}}^C/v_{\text{ex}}^B$ and $v_{\text{ex}}^D/v_{\text{ex}}^B$ by using the intensities of three different spectral bands. This allows the evaluation of the electric field amplitude from Fig. 2.

This procedure requires a knowledge of the atmospheric attenuation, which depends upon the zenith angle, as well as the relative humidity and the aerosol number density. However, if the detector is on a high altitude airplane, the absorption caused by the water vapor and aerosols becomes negligible. Thus, the retrieval procedure is simplified. To illustrate the opportunities given by the proposed method we consider data from Hampton et al. (1996) presented in Fig. 9(a), which only shows the $N_2(1P)$ band. We chose the 6-3 and 7-4 transitions, their intensities relate as 0.62/0.4. We take into account that for the chosen transitions the largest role is played by the direct pumping of the B level and by the

cascade from the B' level. The difference in the atmospheric attenuations, as we check with our model, was less than a few percent for the zenith angle $\chi \sim 80^\circ$. Substituting the ratio of intensities into eqn (6), we obtain that $v_{\text{ex}}^{B'}/v_{\text{ex}}^B \simeq 0.3$; this corresponds to $\tilde{\varepsilon} = 0.1$ eV (or $E_0 = 35$ V/m for $h = 80$ km) according to Fig. 2, which is just below the ionization threshold. Note that this estimate was made using noisy data which are not spatially resolved, and can be considered only as an illustrative example. Thus, in order to retrieve the electric field due to the lightning from observed sprite spectra, some methods such as spectral fitting technique (Green et al. 1996) have to be applied.

3.2. Spatial integration

In order to compare with actual spectrum measurements, we must consider the detector column integration, as photons are emitted from different heights under different conditions, e.g. quiver energies, electron densities, neutral densities, collisional quenching, etc. The column integration, eqn (4), must be carried carefully due to two factors

- the height dependence of the quiver energy, the electron density, and neutral density;
- the height dependence of the collisional quenching.

We can apply the method which we explained above to the electric field induced by a discharge of fractal lightning, as discussed by Valdivia et al. (1997). For definiteness we assume that the lightning has a fractal dimension $D = 1.4$ and is produced by a discharge of $Q = 100C$. We choose the field profile at the core of the sprites to carry out the spatial integration eqn (4). The result is shown in Fig. 10. For this electric field profile,

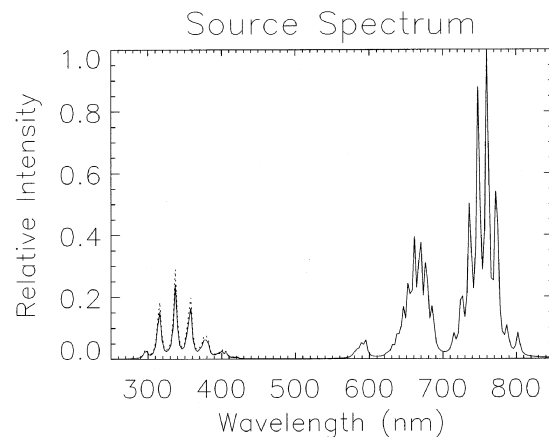


Fig. 10. The spatially integrated source spectrum for a red sprite due to a lightning discharge of $Q = 100C$ (solid line), along with that produced by a slab at 80 km corresponding to $\tilde{\varepsilon} = 0.1$ eV (dashed line).

the relative spectrum does not vary appreciably from the properly normalized spectrum computed for a slab at $h = 80$ km and of $\varepsilon = 0.1$ eV revealed by the dashed line; the difference is only 10% for the short wavelengths belonging to the 2P band and less than 1% for the longer wavelengths of 1P band. Both spectra are plotted together, but for reference they can be compared with the spectrum of Fig. 6. Note that the changes in the spectrum are related to the collisional quenching. We expect that these become more profound for the sprites which spread downward to below 60 km.

4. Conclusions

A model of the red sprite spectrum due to molecular excitation by ionospheric electrons accelerated by the electric field from lightning has been developed. The model allows us to evaluate the electric field amplitude by comparing the intensities of different spectral lines. The model also reveals some differences between aurora and sprite spectra: in the aurora both permitted and forbidden transitions play a noticeable role, while in sprites only permitted transitions are important. Unlike the aurora, the collisions between excited molecules could affect sprites only in a few local spots. Sprites are normally observed at quite a high zenith angle, so that the spectrum is highly influenced by the atmospheric attenuation. It seems that sprites are produced by electrons of much lesser energy than that of auroral electrons. For a given amount of the charge discharged and for an assumed fractal dimension of the lightning, the sprite spectrum can be computed accurately, considering the spatial field distribution and the collisional quenching. As a result, if the measurements have good spatial resolution, the model output could in principle yield the spatial profile of the amplitude of the electric field causing the sprite. By comparison with the observations, the lightning parameters could be evaluated.

Acknowledgements

The work was supported by NSF Grant ATM 9422594. We express our gratitude to A. Gurevich and A. S. Sharma for enlightening discussions. We appreciate the database of the N_2 optical properties provided by R. R. Laher and F. R. Gilmore.

References

Brasseur, G., Solomon, S., 1984. *Aeronomy of the Middle Atmosphere*. Reidel, Norwell, MA.

Cartwright, D.C., 1970. Total cross-sections for the excitation

of the triplet states in molecular nitrogen. *Phys. Rev. A2*, 1331–1347.

Cartwright, D.C., Trajamar, S., Chutjian, A., Williams, W., 1977. Electron impact excitation of the electronic states of N_2 . II. Integral cross-sections at incident energies from 10–50 eV. *Phys. Rev. A16*, 1041–1051.

Cartwright, D.C., 1978. Vibrational populations of the excited states of N_2 under auroral conditions. *J. Geophys. Res. A83*, 517–531.

Freund, R.S., 1971. Electron impact and excitation functions for electronic states of N_2 . *J. Chem. Phys. 54*, 1407–1409.

Gilmore, F.R., Laher, R.R., Espy, P.J., 1992. Franck–Condon factors, r -centroids, electronic transition moments, and Einstein coefficients for many nitrogen and oxygen systems. *J. Phys. Chem. Ref. Data 21*, 1005–1067.

Green, R.D., Fraser, M.E., Rawlins, W.T., 1996. Molecular excitation in sprites. *Geophys. Res. Lett. 23*, 2161–2164.

Greenblatt, G.D., Orlando, J.J., Burkholder, J.B., Ravishankara, A.R., 1990. Absorption measurements of oxygen between 330 and 1140 nm. *J. Geophys. Res. 95*, 18,577–18,582.

Hampton, D.L., Heavner, M.J., Wescott, E.M., Sentman, D.D., 1996. Optical spectral characteristics of sprites. *Geophys. Res. Lett. 23*, 89–92.

Handbook of Chemistry and Physics, 1983–1984. 64th ed. West, R.C. (Ed.). CRC Press, Boca Raton, FL.

Handbook of Geophysics and Space Environment, 1985. 64th ed. Jursa, A.S. (Ed.). Air Force Geophysics Laboratory, U.S. Air Force.

Lenoble, J., 1993. *Atmospheric Radiative Transfer*. A. Deepak, Hampton, Virginia.

Lyons, W.A., 1994. Characteristics of luminous structures in the stratosphere above thunderstorms as imaged by low-light video. *Geophys. Res. Lett. 21*, 875–878.

Mende, S.B., Rairden, R.L., Swenson, G.R., Lyons, W.A., 1995. Sprite Spectra. N_2 1PG Band identification. *Geophys. Res. Lett. 22*, 1633–2636.

Milikh, G.M., Papadopoulos, K., Chang, C.L., 1995. On the physics of high altitude lightning. *Geophys. Res. Lett. 22*, 85–88.

Morill, J.S., Benesh, W.M., 1996. Auroral N_2 emissions and the effect of collisional processes on N_2 triplet state vibrational populations. *J. Geophys. Res. 101*, 261–274.

Nicolet, M., Meier, R.R., Anderson, D.E., 1982. Radiation field in the troposphere and stratosphere. II. Numerical analysis. *Planet. Space Sci. 30*, 935–941.

Pancheshnyi, S.V., Starikovskaya, S.M., Starikovskii, A. Yu., 1997. Measurements of the rates of quenching of $N_2(C^3\Pi_u)$ and $N_2^+(B^2\Sigma_u^+)$ states by N_2 , O_2 and CO molecules in the afterglow plasma of a nanosecond discharge. *Plasma Physics Reports 23*, 615–620.

Pasko, V.P., Inan, U.S., Taranenko, Y.N., Bell, T., 1995. Heating, ionization and upward discharges in the mesosphere due to intense quasi-electrostatic thundercloud fields. *Geophys. Res. Lett. 22*, 365–368.

Rowland, H.L., Fernsler, R.F., Huba, J.D., Bernhardt, P.A., 1995. Lightning driven EMP in the upper atmosphere. *Geophys. Res. Lett. 22*, 361–364.

Sentman, D.D., Wescott, E.M., Osborne, D.L., Hampton, D.L., Heavner, M.J., 1995. Preliminary results from the sprites 94 aircraft campaign, 1, red sprites. *Geophys. Res. Lett. 22*, 1205–1208.

- Tsang, K., Papadopoulos, K., Drobot, A., Vitello, P., Wallace, T., Shanny, R., 1991. RF ionization of the lower ionosphere. *Radio Sci.* 20 (5), 1345–1360.
- Uman, M.A., 1987. *The Lightning Discharge*. Academic Press, Orlando.
- Valdivia, J.A., Papadopoulos, K., Milikh, G.M., 1997. Red sprites: lightning as a fractal antenna. *Geophys. Res. Lett.*, 24, 3169–3172.
- Van Zyl B., Pendleton, W. Jr., 1995. $N_2^+(X)$, $N_2^+(A)$ and $N_2^+(B)$ production in $e^- + N_2$ collisions. *J. Geophys. Res.* 100, 23,755–23,762.
- Winckler, J.R., Lyons, W.A., Nelson, T.E., Nemzek, R.J., 1996. New high-resolution ground-based studies of sprites. *Geophys. Res. Lett.* 191, 6997–7004.